Applied Materials Today 16 (2019) 257–264

Contents lists available at ScienceDirect

Applied Materials Today

journal homepage: www.elsevier.com/locate/apmt

Short communication

Self-supported sulphurized TiO_2 nanotube layers as positive electrodes for lithium microbatteries

Girish D. Salian[a], Milos Krbal[b], Hanna Sopha[b,c], Chrystelle Lebouin[d], Marie-Vanessa Coulet[d], Jan Michalicka[c], Ludek Hromadko[b], Alexander T. Tesfaye[a], Jan M. Macak[b,c], Thierry Djenizian[a,*]

[a] Mines Saint-Etienne, Center of Microelectronics in Provence, Department of Flexible Electronics, F-13541, Gardanne, France
[b] Center of Materials and Nanotechnologies, Faculty of Chemical Technology, University of Pardubice, Nam. Cs. Legii 565, 53002, Pardubice, Czech Republic
[c] Central European Institute of Technology, Brno University of Technology, Purkyňova 123, 612 00, Brno, Czech Republic
[d] Aix-Marseille University, CNRS, MADIREL, UMR 7246, Marseille, France

ARTICLE INFO

Article history:
Received 4 March 2019
Received in revised form 22 May 2019
Accepted 30 May 2019

Keywords:
Titania nanotubes
Sulphurization
Self-supported
Cathode
Li-ion microbatteries

ABSTRACT

We report the synthesis and characterization of self-supported sulphurized TiO_2 nanotube layers as a cathode material for Li microbatteries. Sulphurized TiO_2 nanotubes were obtained by annealing of self-supported TiO_2 nanotubes in sulphur atmosphere. The morphology, structure, composition and thermal stability of the $Ti_xO_yS_z$ nanotube layers were studied by scanning electron microscopy, transmission electron microscopy, X-ray diffraction, X-ray photoelectron spectroscopy and thermogravimetric analysis. The electrochemical behaviors of the chemically modified nanotubes were investigated by cyclic voltammetry and chronopotentiometry techniques. This nanostructured electrode used as a cathode material showed high rate capabilities even at very fast kinetics. Remarkably, a high discharge capacity (340 $\mu Ah\,cm^{-2}$) has been retrieved after 100 cycles with 100% coulombic efficiency attesting the excellent stability of the electrode.

1. Introduction

The development of modern microelectronic devices like microelectromechanical systems (MEMS), Radio Frequency Identification (RFID) tags, medical implants, or smart cards, have necessitated the need of microscale power sources [1–5]. These microscale power sources must not only be miniaturized but also fulfill the energy and the power density requirements of the devices. Lithium batteries have been characterized by higher energy per unit weight of the known energy storage systems and hence they can be miniaturized to be integrated in microelectronic devices [2]. However, the electrochemical performance of 2D microbatteries composed of planar thin-films cannot feed a variety of low power devices. In this context, self-supported 3D nanoarchitectures are expected to offer several advantages for microbatteries such as short transport length of charges, interpenetration between active components, and small areal footprints [6–9]. Pristine and chemically modified self-supported TiO_2 nanotube layers (TNTs) have been extensively explored as anodes for Li-ion microbatteries [2,9–24].

TNTs have also been reported to be good intercalation hosts for sulphur [25,26]. Sulphur as a cathode material possesses a high theoretical capacity of 1675 $mAh\,g^{-1}$ and hence a high energy density making a very good candidate for lithium-sulphur (Li-S) batteries [27–30]. However, there are some limitations associated with Li-S batteries like poor conductivity of sulphur, short cycle life, low cycling efficiency, or huge capacity fade mainly due to the dissolution of the active material in the electrolyte [27]. To overcome these problems, transition metal sulphides such as TiS_2 and TiS_3 have been studied as positive electrodes for Li batteries [31–35]. In general, transition metal sulphides exhibit high electrical conductivity and low solubility in electrolytes [36–38]. These properties represent a clear advantage over elemental sulphur. The theoretical capacity of crystalline TiS_3 (556 $mAh\,g^{-1}$) is higher than that of TiS_2 (240 $mAh\,g^{-1}$) [39,40]. Lindic et al. found that the TiS_3 containing TiO_xS_y thin-films exhibited higher areal capacities for the initial few cycles but suffered from high capacity fade [35]. Hayashi et al. reported that amorphous TiS_3 particles have a high reversible capacity of 400 $mAh\,g^{-1}$ in all-solid-state batteries [41]. Self-supported TNTs containing TiS_3 phase was reported by Kyerematang et al. [34]. The electrode delivered good initial areal capacities but a huge continuous capacity fade has been observed during cycling tests. Actually, the stability of the discharge capacities delivered by the cathode material was poor with a capacity

* Corresponding author.
E-mail address: thierry.djenizian@emse.fr (T. Djenizian).

https://doi.org/10.1016/j.apmt.2019.05.015

fade in a matter of 50 cycles. The origin of the degradation was attributed to the eventual structural distortion of the material as the catholyte formation has not been evidenced.

In the present study, we report that remarkable electrochemical performance of sulphurized TNTs can be obtained. We overcome the capacity fading due to structural distortion problem by controlling the synthesis parameters during the sulphurization treatment. The resultant sulphurized nanotubes deliver excellent areal capacities with good stability of the discharge capacities up to 100 cycles even at fast kinetics making sulphurized TNTs a potential candidate as a positive electrode for Li microbatteries.

2. Materials and methods

2.1. Synthesis of TNTs and sulphurized TNTs

The TNTs were obtained by anodizing Ti substrates. Prior to anodization, the Ti foils (127 μm thick, Sigma-Aldrich) were degreased by sonication in isopropanol and acetone for 1 min each, then rinsed in isopropanol and dried in air. The electrochemical setup consisted of a two-electrode configuration using a platinum foil as the counter electrode, while the Ti foils (working electrodes) were pressed against an O-ring of the electrochemical cell, leaving 1 cm^2 open to the electrolyte that consisted of ethylene glycol containing 176 mM NH_4F and 1.5 vol% H_2O [42]. The electrolyte was prepared from reagent grade chemicals. Before use, the electrolyte was aged for 9 h by anodization of blank Ti substrates at 60 V under the same conditions as for the main anodization experiments [43]. Electrochemical experiments were carried out at room temperature employing a high-voltage potentiostat (PGU–200 V, IPS Elektroniklabor GmbH). The anodization was carried out at 60 V for 4 h with an initial sweeping rate of 1 V s^{-1}. After the anodization the TNTs were rinsed and sonicated in isopropanol for 5 min and dried in air. The as-obtained pristine TNTs being amorphous, they were afterward annealed in a muffle oven (400 °C, 1 h) to obtain anatase structure. In the next step, TNTs along with 0.2 g of pure sulphur were placed into pre-cleaned quartz ampoules which were subsequently evacuated to 10^{-3} Pa and sealed. The evacuated ampoules were heated at 400 °C for 3 h, and then naturally cooled to room temperature inside the furnace. The temperature was increased with a rate of 5 °C min^{-1}. The sulphurized TNT layers are designated as S-TNTs.

2.2. Material characterizations

The morphology of the pristine TNTs and S-TNTs were characterized by a field-emission SEM (FE SEM JEOL JSM 7500F) and a high-resolution transmission electron microscope (FEI Titan Themis 60-300, operated at 300 keV) equipped with a high angle annular dark field (HAADF) detector (Fischione) for scanning transmission electron microscopy (STEM) imaging and with energy dispersive X-ray (EDX) spectroscope (FEI SUPER-X) with 4×30 mm^2 windowless silicon drift detectors. The cross-sectional views were taken from mechanically bent samples or scratched samples by scalpel. The bending process led to the rupture of the nanotube layers, enabling to visualize even individual nanotubes in various details. Diffraction analyses of the S-TNTs were carried out using X-ray diffractometer (XRD, D8 Advance, Bruker AXE) to determine the different phases present in the material using Cu Kα (λ = 1.54 Å) radiation equipped with a secondary graphite monochromator and Na (Tl) I scintillation detector. The chemical composition of S-TNTs was determined by ultra-high vacuum (UHV, base pressure below 1×10^{-9} mbar) X-ray photoelectron spectroscopy (XPS, ESCA 2SR, Scienta-Omicron) using monochromatic Al Kα source (1486.6 eV). The XPS was performed on the S-TNT powder scratched out from the S-TNT layer in order to average signal over entire depth of S-TNT layer. The stability of the S-TNTs was monitored using thermogravimetric analysis (TGA). The measurements were done using a Q500 apparatus from TA Instrument. In order to avoid any oxidization, the S-TNTs were heated under Ar atmosphere and a heating rate of 5 °C min^{-1} was applied from ambient temperature up to 600 °C.

2.3. Electrochemical measurements

The electrochemical performance of the pristine TNTs and S-TNTs were studied using Swagelok-type cells. For the galvanostatic charge/discharge cycling tests, pristine TNTs and S-TNTs were assembled in a two-electrode configuration with a metallic Li foil (Aldrich) as the counter electrode and a glass fiber (Whatman) soaked in the electrolyte used as the separator. The electrolyte consisted of a solution of 1 M $LiPF_6$ in ethylene carbonate (EC)/diethyl carbonate (DEC) (1:1, in w/w) (Sigma-Aldrich). For the cyclic voltammetry tests, pristine TNTs and S-TNTs were assembled in a three-electrode system with two Li foils acting respectively as reference and counter electrodes and separated by a Whatman paper soaked in EC:DEC with 1 M $LiPF_6$. The cells were assembled in an argon-filled glovebox (MBraun, Germany), with <0.5 ppm H_2O and <0.5 ppm O_2 atmosphere. The cyclic voltammetry and galvanostatic charge/discharge tests were carried out using a VMP3 potentiostat (Bio Logic, France). The CV curves were recorded in a potential window of 1–3 V *vs.* Li/Li^+ at a scan rate of 0.1 mV s^{-1}, both for pristine TNTs and S-TNTs Galvanostatic charge/discharge tests were performed at multiple C-rates in the potential window of 1–3 V *vs.* Li/Li^+.

3. Results and discussions

Fig. 1a and b shows the SEM images of the top and cross-sectional views of the pristine TNTs. The nanotubes were characterized by an outer diameter of ~145 nm, an inner diameter of ~135 nm and the wall thickness of ~5 nm at the top of the nanotube layers. Due to the conical shape of the nanotubes, however, the tube wall gets thicker and the inner nanotube diameter gets smaller in deeper parts of the nanotube layer, as shown in our previous work [42]. The thickness of the nanotube layers was ~15 μm. Fig. 1c shows the top view of S-TNTs. As observed from the SEM image, the sulphur deposition forms a thick layer on the nanotubes along the rim of the nanotube walls. The thickness of this layer is ~35 nm. However, the nanotubular morphology is preserved after the heat treatment in the sulphur atmosphere, which is apparent from SEM images in Fig. 1c and d, and in a detailed STEM-HAADF image of a fragment of S-TNTs shown in Fig. 1e. In addition, as apparent from the STEM-EDX elemental map, the composition of the S-TNT is very uniform along the walls, with S species evenly distributed within the TNT walls (see Fig. S1 for more details).

The structure of S-TNTs has been investigated by XRD analysis. The XRD pattern given in Fig. 2a reveals the presence of two phases, *i.e.* anatase TiO_2 and TiS_3 (formula $Ti^{4+}S_2^{2-}S^{2-}$). However, the presence of TiS_2 in the material cannot be excluded as it could be present in the amorphous form at this temperature [35,39,40]. The Ti peaks stem from the underlying Ti substrate. In order to have a better insight into the chemical composition of the material, the chemical state of S-TNT surface was examined by XPS. The S 2p and Ti 2p spectra are shown in Fig. 2b. S 2p spectrum consisted of two doublets at 160.2 eV and 161.5 eV assigned to sulfide S^{2-} and disulfide pairs S_2^{2-}, respectively. The ratio of S_2^{2-} to S^{2-} doublet areas was found to be 1.2, which corresponded to 3:2 ratio of TiS_3 to TiS_2, respectively [44]. The formation of TiS_x was also reflected in the Ti 2p spectrum (inset of Fig. 2c) by the doublet at 455.3 eV.

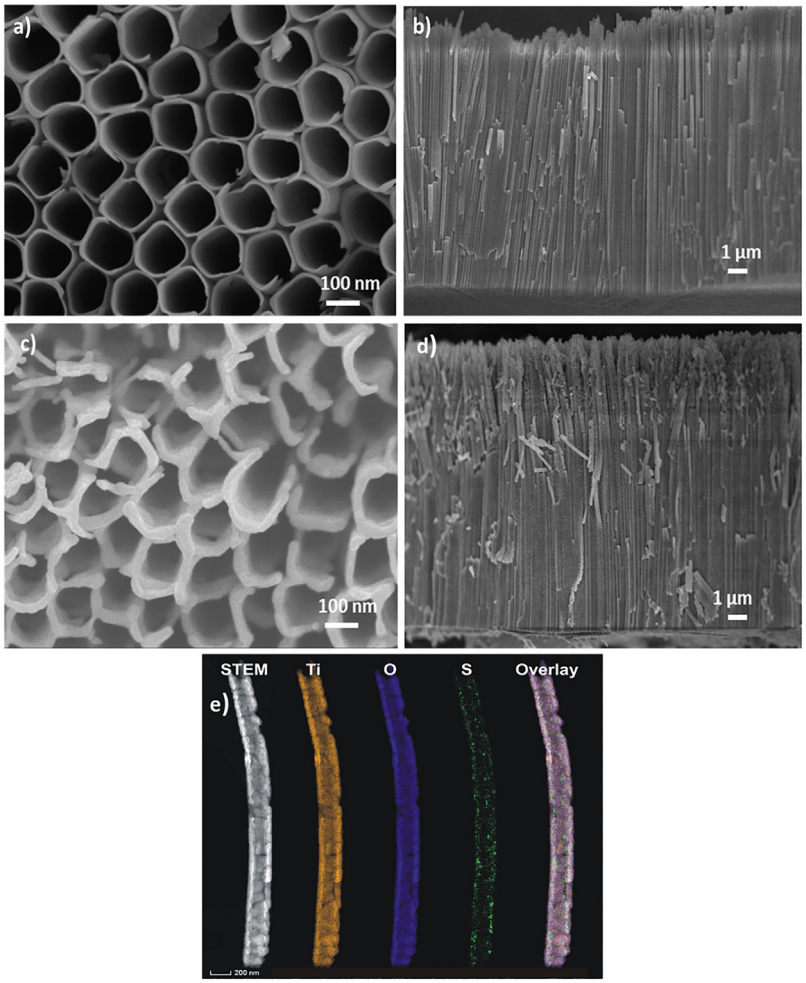

Fig. 1. SEM images of the pristine TNTs (a) top view and (b) cross-sectional view; the S-TNTs (c) top view and (d) cross-sectional view; (e) STEM-HAADF image and STEM-EDX elemental maps of a fragment of the S-TNTs.

The presence of elemental sulphur could not be verified because it was not stable under UHV conditions. No higher oxidation states of sulphur were detected. The stability of the S-TNT is illustrated on the TGA thermogramm given in Fig. 2c. It has to be noted that the weight losses are normalized in respect with the estimated mass of nanotubes. The analysis reveals two weight loss stages. The first one is about 2.4% and occurs between 150 and 200 °C. It is attributed to the evaporation of a small amount sulphur as confirmed by the TGA curve for pure sulphur [45]. This result suggests that unreacted sulphur was present in the sample, either trapped inside the nanotubes or adsorbed at the surface. The fact that sulphur was not observed in XRD pattern may be attributed to its amorphous nature resulting from the sulphurization process. The second weight loss stage starts around 300 °C and corresponds to a weight loss equal to 16.9%. It can be attributed to the decomposition of TiS_3 phase into TiS_2 [46,47].

The electrochemical behavior of pristine TNTs and S-TNTs sample were studied by cyclic voltammetry (Fig. 3a and c). The reduction peak at 1.75 V *vs.* Li/Li^+ and the oxidation peak at 2.1 V *vs.* Li/Li^+ correspond to the Li^+ insertion/extraction into/from the anatase phase present in both samples, according to Eq. (1) [8,11–13]. Additionally the area under the CV curve for the S-TNTs is higher than the pristine TNTs suggesting higher electron transfers. Examination of the CVs up to the 10th cycle for S-TNTs reveals the presence of peaks typical for several reactions with Li ions for S-TNTs. The presence of good reversibility is achieved by demonstrating an overlap in sweeps.

$$TiO_2 + xLi^+ + xe^- \leftrightarrow Li_xTiO_2 \quad \text{for} \quad 0 \leq x \leq 1 \tag{1}$$

Then, other reversible broad anodic/cathodic peaks observed at potentials higher than 2.1 V are due to the presence of S in the form of sulphides as it has been reported for $Ti_xO_yS_z$ thin films [35]. Hence, $Ti_xO_yS_z$ can react with Li ions according to Eq. (2).

$$Ti_xO_yS_z + nLi^+ + ne^- \leftrightarrow Li_nTi_xO_yS_z \quad \text{for} \quad 0 \leq n \leq 1 \tag{2}$$

However, two cathodic peaks at 1.9 V and 2.1 V appearing only in the first cycle can be attributed to the irreversible reaction of TiS_3 with Li^+. Actually, TiS_3 reacts with up to 3 Li^+ per formula unit (2 Li^+ react irreversibly) in a two-step intercalation mechanism according to Eqs. (3) and (4) [33,34].

$$TiS_3 + 2Li^+ + 2e^- \rightarrow Li_2TiS_3 \tag{3}$$

$$Li_2TiS_3 + xLi^+ + xe^- \leftrightarrow Li_{2+x}TiS_3 \quad \text{for} 0 \leq x \leq 1 \tag{4}$$

In Eq. (3), the $[S_2^{2-}]$ bonds present in TiS_3 are broken during the insertion of Li^+ into the structure resulting in the reduction of S_2^{2-}. This irreversible reaction leads to a change in the titanium coordination polyhedron from trigonal prismatic to the more stable octahedron geometry [33]. The next reaction (Eq. (4)) which is reversible, takes place during the insertion of the third Li^+ in Li_2TiS_3

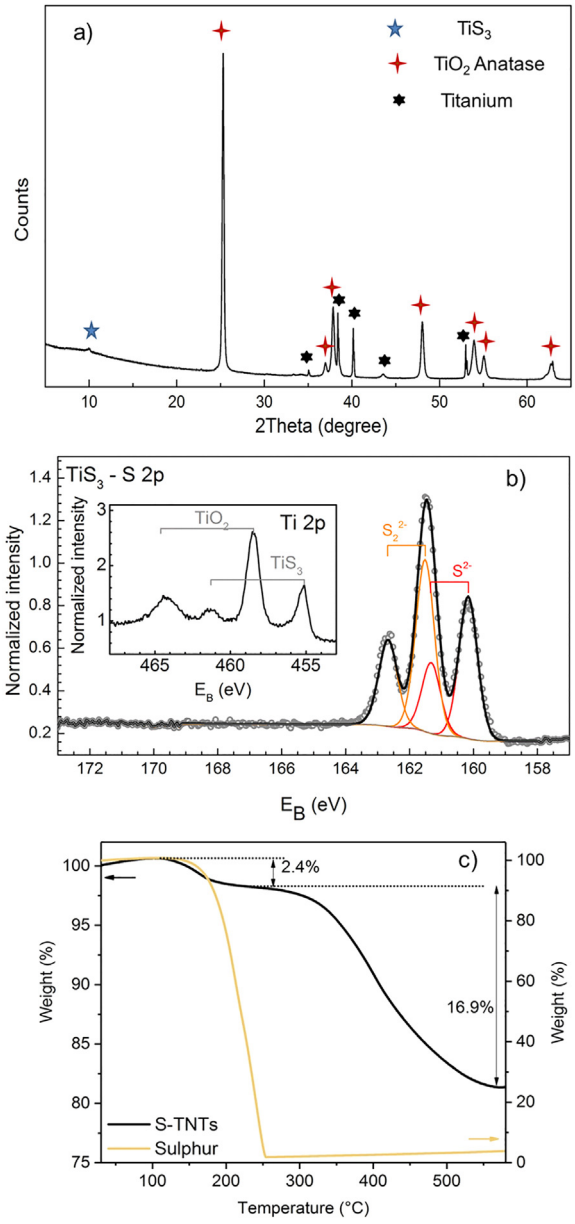

Fig. 2. (a) XRD pattern of S-TNTs sample; (b) XPS S 2p and Ti 2p (inset) spectra of S-TNTs sample; (c) TGA curves for S-TNTs sample and pure Sulphur recorded in Ar atmosphere with a heating rate of 5 °C min^{-1}.

at a potential of around 2.3 V as it has been confirmed by the large cathodic peak visible after the first cycle. Disordered TiS_2 could also react with up to 1 Li^+ per formula unit reversibly according to Eq. (5) [35,40].

$$TiS_2 + Li^+ + e^- \leftrightarrow LiTiS_2 \quad (5)$$

It can be noticed that the presence of a cathodic plateau between 2.2 and 1.8 V can be ascribed to a pseudocapacitive effect, which is typical for nano domains [48]. González et al. showed that shorter nanotubes contributed to the additional capacity due to large area exposed to the electrolyte [49]. Whiteley et al. reported that disordered $LiTiS_2$ composed of nanocristallites showed additional charge storage derived by reducing surface Ti^{3+} to Ti^{2+} at higher voltages and more reversibly than traditionally shown [50].

Galvanostatic charge/discharge tests were performed on the pristine TNTs and S-TNTs samples in half-cell (*vs.* Li/Li^+) configuration. The current was applied based on TNTs assuming a porosity of 78%. The porosity calculation is based on the amount of the TiO_2 nanotubes per cm^2. The volume of the TNTs was calculated by subtracting the inner tube area from outer tube area. Fig. 3b and d shows the galvanostatic charge/discharge curves of the electrodes at a current density of 34 μA cm^{-2} (C/10) for the pristine TNTs and S-TNTs respectively. Each cycle shows the presence of characteristic plateaus that are consistent with the peaks obtained from the CV curves. The first cycle delivers a discharge capacity of 342 μAh cm^{-2} (70 mAh g^{-1}) and 748 μAh cm^{-2} (197 mAh g^{-1}) for the pristine TNTs and S-TNTs, respectively. The first irreversible capacity is a characteristic of the TiO_2 based electrodes due to the reaction of Li ions with structural defects and the residual water [9,51,52]. Possible ways to mitigate this irreversible capacity has been suggested by Brutti et al., wherein TiO_2 has been pre-lithiated by adding nano-lithium powder [53]. The 10th cycle gives a discharge capacity of 285 μAh cm^{-2} (51 mAh g^{-1}) and 578 μAh cm^{-2} (152 mAh g^{-1}) for the pristine TNTs and S-TNTs respectively. Clearly the discharge capacities for the S-TNTs are higher than their pristine counterparts suggesting that the capacities in S-TNTs are contributed both

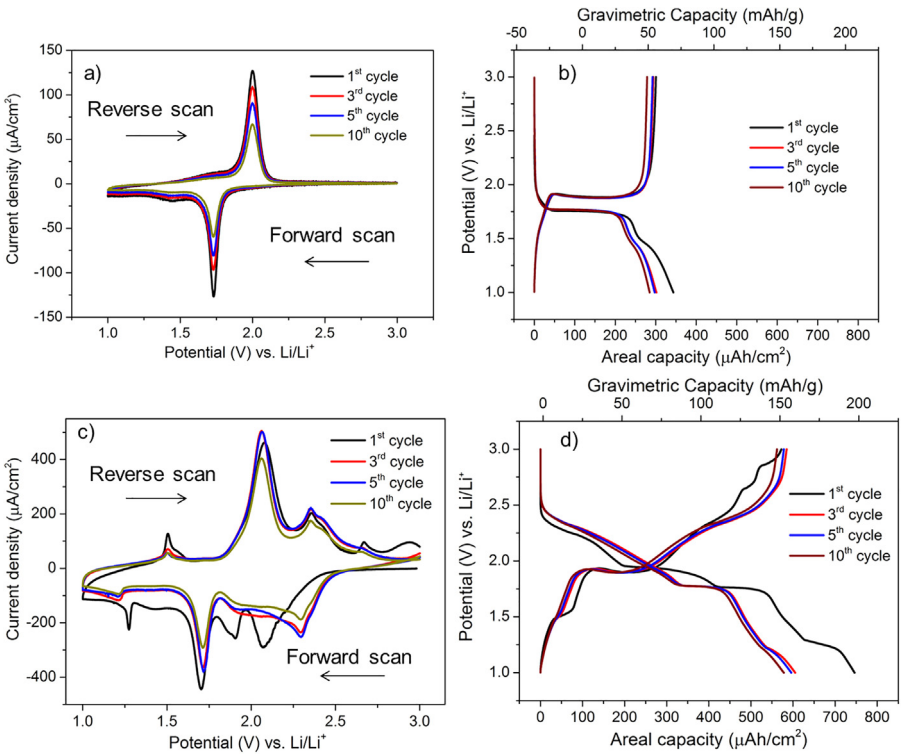

Fig. 3. (a) Cyclic voltammetry curves of the pristine TNTs sample at a scan rate of 0.1 mV s^{-1}; (b) galvanostatic charge/discharge curves of the pristine TNTs at C/10 rate; (c) cyclic voltammetry curves of the S-TNTs sample at a scan rate of 0.1 mV s^{-1}; (d) galvanostatic charge/discharge curves of the S-TNTs at C/10 rate. The potential range for both CV and Galvanostatic tests were 1–3 V *vs.* Li/Li^+.

by anatase and the titanium sulphides. The operating voltage of the S-TNTs sample is 2.3 V suggesting that it is a potential positive electrode for lithium metal batteries.

Fig. 4a shows the long-term cycling behavior of the pristine TNTs and S-TNTs sample for 100 cycles at a current density of 340 μA cm^{-2} (1C). The discharge capacities for the S-TNTs are remarkably higher than the pristine TNTs suggesting that the enhanced discharge capacity of S-TNTs is due to the contribution of the anatase and the titanium sulphide phases.

The cycle behavior for the S-TNTs shows stable capacities up to 100 cycles with 100% coulombic efficiency (Fig. 4b). The 100th cycle delivered a discharge capacity of 400 μAh cm^{-2}. The capacity retention between the first reversible cycle (2nd cycle) and the 100th cycle is 93%. These results show the excellent electrochemical behavior of the S-TNTs. To investigate further on the rate performance of the S-TNTs, the cell was cycled at higher current densities (Fig. 4a). The electrode delivers discharge capacity values of ~543 μAh cm^{-2} (145 mAh g^{-1}) at 68 μA cm^{-2} (C/5), ~430 μAh cm^{-2} (110 mAh g^{-1}) at 340 μA cm^{-2} (1C), ~300 μAh cm^{-2} (78 mAh g^{-1}) at 680 μA cm^{-2} (2C), ~170 μAh cm^{-2} (46 mAh g^{-1}) at 1.7 mA cm^{-2} (5C). The electrode shows high rate capabilities at very fast kinetics. More remarkably, the discharge capacities are retrieved after cycling at very high current densities attesting the excellent stability of the material compared to previous work [34].

Origins of the high discharge capacity and the outstanding stability during cycling tests may have two explanations. Firstly, according to the first cycle, sulphur ions mainly contribute to the electrochemical processes. Lindic et al. suggested that the TiO_xS_y films delivering good cycle stability showed the reduction of the disulphide bonds were more reversible than the films which gave poor cycle stability [33]. The same reason could be attributed in the present study. Secondly, the same research group suggested that the capacity fading is mainly attributed to the structural distortions during the reaction with lithium. The S-TNTs sample in the present study portrays good cycling stability, which indicates that structural distortions are not present and that the structure is therefore more stable. When we compare the results of the previous reports for the S-TNTs by Kyeremetang et al. [34], the areal capacities herein are higher and additionally the discharge capacities up to 100 cycles is stable. Probably the structural distortion in the TiO_xS_y nanotubes from the previous study, comes from the fact that the formation of this phase was faster during the heat treatment (200 °C min^{-1}), which could render the phase less crystalline with more structural distortions and defects. Whereas in the present study, the heat treatment in the sulphur atmosphere was done at 5 °C min^{-1}, a much slower rate for which the material has ample time to form stable phases with less structural distortions.

Post-mortem analysis was performed after 100 cycles. The cell after the cycling test was disassembled to retrieve the electrode. Fig. 5 a and b shows the SEM images of the cycled sample. In comparison with SEM images of the S-TNTs before cycling (Fig. 1c and d), there is no major degradation and the nanotubular morphology is preserved. Fig. 5 c and d shows the XRD diffractogram recorded on the S-TNT sample tested after 100 cycles. In agreement with the electrochemical tests, the TiS_3 peak actually disappeared while an additional small peak confirms the formation of the Li_2TiS_3 and $LiTiS_2$ phases (Fig. 5d). Even remarkably, another peak corresponding to the appearance of $LiTiO_2$ is observed in the diffractogram. Such inactive LTO from an electrochemical point of view may contribute to the stabilization of the electrode as it has been reported elsewhere [53]. In order to clarify the electrochemical reaction of the S-TNT electrode with Li ions, XPS measurements have been performed after the 2nd charge and the 3rd discharge. The resulting S 2p XPS spectra of S-TNTs samples are shown in Fig. 5e. The charge and discharge cycles were accompanied by the deacrease of TiS_3 content relative to TiS_2 and by a partial surface oxidation of sulfides. The ratio of S_2^{2-} to S^{2-} doublet area dropped from 1.2 to 0.3

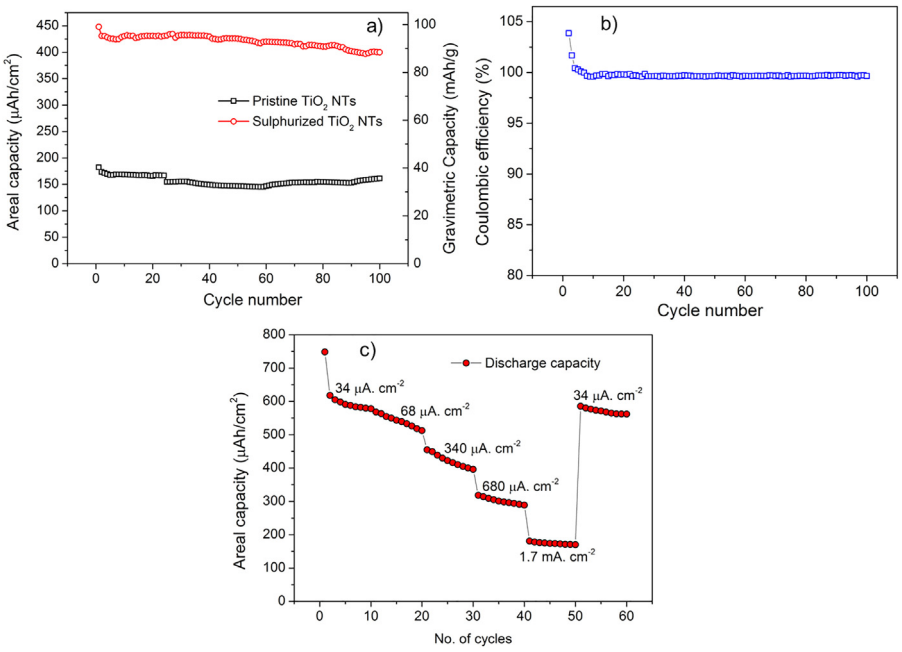

Fig. 4. (a) Long term cycling tests of pristine TNTs and S-TNTs sample for 100 cycles at a current density of 340 μA cm^{-2} (1C rate); (b) coulombic efficiency of the S-TNTs sample for 100 cycles; (c) electrochemical performance of S-TNTs at various current densities (C rates).

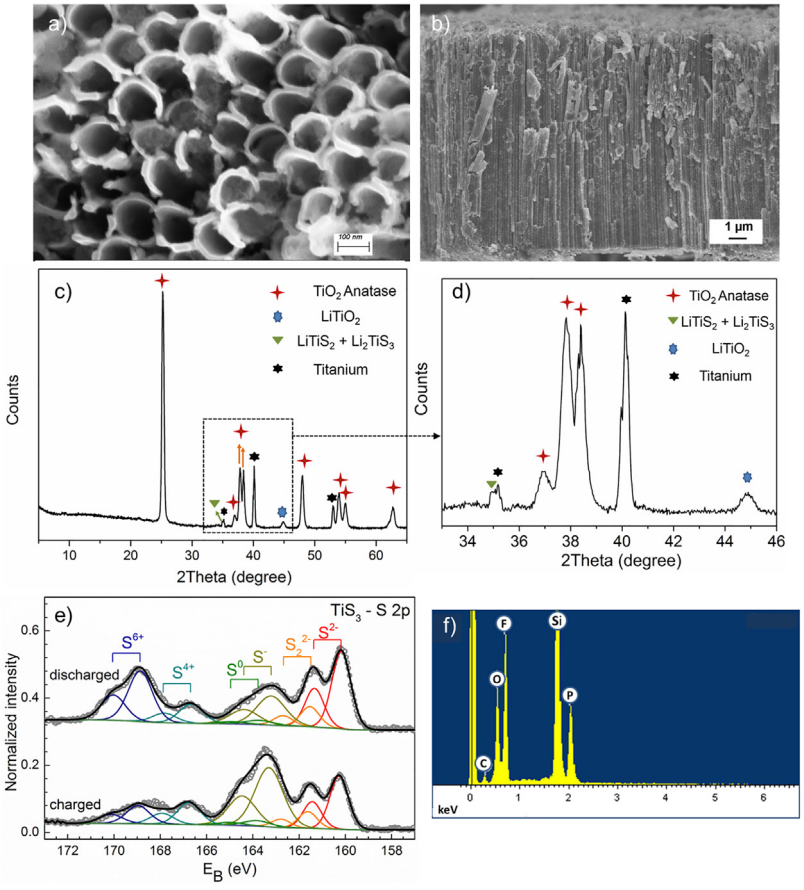

Fig. 5. SEM images of the S-TNTs sample post long-term cycling tests for 100 cycles (a) top view; (b) cross-sectional view; (c) XRD diffractogram of the cycled sample; (d) zoomed image of the XRD diffractogram; (e) S 2p XPS spectra of S-TNTs after 2nd charge and 3rd discharge; (f) EDX spectrum analysis of the electrolyte retrieved from the cell.

featuring the 1:7 TiS_3 to TiS_2 ratio confirming the reactions mentioned above. The oxidation states of S^{-}, S^{4+}, and S^{6+} were observed in S 2p spectra as doublets at 163.2, 166.7, and 168.8 eV in both charged and the discharged state of the electrode. This results suggests the formation of a SEI-like layer probably composed of a mixture of LiS, Li_2SO_3, and Li_2SO_4 that could be responsible for the initial capacity fading. A post-mortem EDX spectrum analysis (Fig. 5f) of the electrolyte retrieved from the cell after the 100 cycles revealed only the presence of P, C, F and O elements indicating that there was no sulphur dissolution into the electrolyte (Si signal is detected because the electrolyte was dried at room temperature on a Si substrate).

4. Conclusions

Self-supported sulphurized TiO_2 nanotube layers were investigated as potential positive electrodes for Li microbatteries. The morphology of the sulphurized TNTs revealed that the chemical treatment has not altered the morphology of the titania nanotubes. Additionally, the STEM-EDX analysis confirmed the uniform distribution of sulphur within the nanotubes. The chemical characterization experiments revealed the presence of anatase TiO_2 and TiS_3 phases. According to the galvanostatic cycling tests, the $Ti_xO_yS_z$ nanotubes delivered an average areal capacity of 600 $\mu Ah\,cm^{-2}$ at C/10 rate with coulombic efficiencies of 100% and a capacity retention between the 2nd and the 100th cycle of 93% compared to their pristine counterparts. The rate performance of the electrodes delivered stable capacity values even at very fast kinetics (170 $\mu Ah\,cm^{-2}$ at 5C rate) and the long-term cycling tests up to 100 cycles showed remarkable stability compared to the previous reports. The *post-mortem* analysis revealed that the nanotubular morphology is not affected and the phases of TiS_3 and TiS_2 are retained after cycling. The EDX analysis shows no dissolution of Sulphur after cycling and XPS analysis suggest the formation of a SEI-like layer composed of lithium sulfides that could be responsible for the initial capacity fading. The reasons for the excellent electrochemical behaviors can be attributed to the optimized thermal parameters for the fabrication of $Ti_xO_yS_z$ nanotubes and the formation of inactive $LiTiO_2$ improving the structural stability of the electrode.

Acknowledgments

The authors gratefully acknowledge the European Research Council (project No. 638857) and the Ministry of Education, Youth and Sports of the Czech Republic (projects LM 2015041, LM2015082, LQ1601 and CZ.02.1.01/0.0/0.0/16_013/0001829) for financial support of this work, whose part was carried out with the support of CEITEC Nano Research Infrastructure. This work has been carried out thanks to the support of the A*MIDEX project (*n° ANR-11-IDEX-0001-02*) funded by the Ïnvestissements d'Avenir" French government program, managed by the French National Research Agency (ANR).

Appendix A. Supplementary data

Supplementary data associated with this article can be found, in the online version, at doi:10.1016/j.apmt.2019.05.015.

References

[1] S. Ferrari, M. Loveridge, S.D. Beattie, M. Jahn, R.J. Dashwood, R. Bhagat, Latest advances in the manufacturing of 3D rechargeable lithium microbatteries, J. Power Sources 286 (2015) 25–46, http://dx.doi.org/10.1016/j.jpowsour.2015.03.133.
[2] B.L. Ellis, P. Knauth, T. Djenizian, Three-dimensional self-supported metal oxides for advanced energy storage, Adv. Mater. 26 (2014) 3368–3397, http://dx.doi.org/10.1002/adma.201306126.
[3] J.F.M. Oudenhoven, L. Baggetto, P.H.L. Notten, All-solid-state lithium-ion microbatteries: a review of various three-dimensional concepts, Adv. Energy Mater. 1 (2011) 10–33, http://dx.doi.org/10.1002/aenm.201000002.
[4] M. Roberts, P. Johns, J. Owen, D. Brandell, K. Edstrom, G. El Enany, C. Guery, D. Golodnitsky, M. Lacey, C. Lecoeur, H. Mazor, E. Peled, E. Perre, M.M. Shaijumon, P. Simon, P.L. Taberna, 3D lithium ion batteries–from fundamentals to fabrication, J. Mater. Chem. 21 (2011) 9876–9890, http://dx.doi.org/10.1039/c0jm04396f.
[5] Y. Wang, B. Liu, Q. Li, S. Cartmell, S. Ferrara, Z.D. Deng, J. Xiao, Lithium and lithium ion batteries for applications in microelectronic devices: a review, J. Power Sources 286 (2015) 330–345, http://dx.doi.org/10.1016/j.jpowsour.2015.03.164.
[6] L. Baggetto, H.C.M. Knoops, R.A.H. Niessen, W.M.M. Kessels, P.H.L. Notten, 3D negative electrode stacks for integrated all-solid-state lithium-ion microbatteries, J. Mater. Chem. 20 (2010) 3703–3708, http://dx.doi.org/10.1039/b926044g.
[7] S.K. Cheah, E. Perre, M. Rooth, M. Fondell, A. Hårsta, L. Nyholm, M. Boman, T. Gustafsson, J. Lu, P. Simon, K. Edström, Self-supported three-dimensional nanoelectrodes for microbattery applications, Nano Lett. 9 (2009) 3230–3233, http://dx.doi.org/10.1021/nl9014843.
[8] G.F. Ortiz, I. Hanzu, P. Knauth, P. Lavela, J.L. Tirado, T. Djenizian, TiO_2 nanotubes manufactured by anodization of Ti thin films for on-chip Li-ion 2D microbatteries, Electrochim. Acta 54 (2009) 4262–4268, http://dx.doi.org/10.1016/j.electacta.2009.02.085.
[9] G.D. Salian, C. Lebouin, A. Demoulin, M.S. Lepihin, S. Maria, A.K. Galeyeva, A.P. Kurbatov, T. Djenizian, Electrodeposition of polymer electrolyte in nanostructured electrodes for enhanced electrochemical performance of thin-film Li-ion microbatteries, J. Power Sources 340 (2017) 242–246, http://dx.doi.org/10.1016/j.jpowsour.2016.11.078.
[10] N. Plylahan, M. Letiche, M.K. Samy Barr, B. Ellis, S. Maria, T.N.T. Phan, E. Bloch, P. Knauth, T. Djenizian, High energy and power density TiO_2 nanotube electrodes for single and complete lithium-ion batteries, J. Power Sources 273 (2015) 1182–1188, http://dx.doi.org/10.1016/j.jpowsour.2014.09.152.
[11] H. Sopha, G.D. Salian, R. Zazpe, J. Prikryl, L. Hromadko, T. Djenizian, J.M. Macak, ALD Al_2O_3-coated TiO_2 nanotube layers as anodes for lithium-ion batteries, ACS Omega 2 (2017) 2749–2756, http://dx.doi.org/10.1021/acsomega.7b00463.
[12] N.A. Kyeremateng, F. Vacandio, M.T. Sougrati, H. Martinez, J.C. Jumas, P. Knauth, T. Djenizian, Effect of Sn-doping on the electrochemical behaviour of TiO_2 nanotubes as potential negative electrode materials for 3D Li-ion micro batteries, J. Power Sources 224 (2013) 269–277, http://dx.doi.org/10.1016/j.jpowsour.2012.09.104.
[13] G.D. Salian, B.M. Koo, C. Lefevre, T. Cottineau, C. Lebouin, A.T. Tesfaye, P. Knauth, V. Keller, T. Djenizian, Niobium alloying of self-organized TiO_2 nanotubes as an anode for lithium-ion microbatteries, Adv. Mater. Technol. 3 (2018), http://dx.doi.org/10.1002/admt.201700274.
[14] N. Plylahan, M. Letiche, M.K.S. Barr, T. Djenizian, All-solid-state lithium-ion batteries based on self-supported titania nanotubes, Electrochem. Commun. 43 (2014) 121–124, http://dx.doi.org/10.1016/j.elecom.2014.03.029.
[15] G. Du, Z. Guo, P. Zhang, Y. Li, M. Chen, D. Wexler, H. Liu, SnO_2 nanocrystals on self-organized TiO 2 nanotube array as three-dimensional electrode for lithium ion microbatteries, J. Mater. Chem. 20 (2010) 5689–5694, http://dx.doi.org/10.1039/c0jm00330a.
[16] Q. Zhu, H. Hu, G. Li, C. Zhu, Y. Yu, TiO_2 nanotube arrays grafted with MnO2 nanosheets as high-performance anode for lithium ion battery, Electrochim. Acta 156 (2015) 252–260, http://dx.doi.org/10.1016/j.electacta.2015.01.023.
[17] L. Gao, H. Hu, G. Li, Q. Zhu, Y. Yu, Hierarchical 3D TiO_2@Fe_2O_3 nanoframework arrays as high-performance anode materials, Nanoscale 6 (2014) 6463–6467, http://dx.doi.org/10.1039/c4nr00387j.
[18] D. Fang, K. Huang, S. Liu, Z. Li, Electrochemical properties of ordered TiO_2 nanotube loaded with Ag nano-particles for lithium anode material, J. Alloys Compd. 464 (2008) L5, http://dx.doi.org/10.1016/j.jallcom.2007.09.141.
[19] Y. Fan, N. Zhang, L. Zhang, H. Shao, J. Wang, J. Zhang, C. Cao, Co_3O_4-coated TiO_2 nanotube composites synthesized through photo-deposition strategy with enhanced performance for lithium-ion batteries, Electrochim. Acta 94 (2013) 285–293, http://dx.doi.org/10.1016/j.electacta.2013.01.114.
[20] Y. Zhao, W. Zhu, G.Z. Chen, E.J. Cairns, Polypyrrole/TiO_2 nanotube arrays with coaxial heterogeneous structure as sulfur hosts for lithium sulfur batteries, J. Power Sources 327 (2016) 447–456, http://dx.doi.org/10.1016/j.jpowsour.2016.07.082.
[21] J. Brumbarov, J. Kunze-Liebhäuser, Silicon on conductive self-organized TiO_2 nanotubes-a high capacity anode material for Li-ion batteries, J. Power Sources 258 (2014) 129–133, http://dx.doi.org/10.1016/j.jpowsour.2014.02.049.
[22] M. Madian, L. Giebeler, M. Klose, T. Jaumann, M. Uhlemann, A. Gebert, S. Oswald, N. Ismail, A. Eychmüller, J. Eckert, Self-organized TiO_2/CoO nanotubes as potential anode materials for lithium ion batteries, ACS Sustain. Chem. Eng. 3 (2015) 909–919, http://dx.doi.org/10.1021/acssuschemeng.5b00026.
[23] S.H. Kim, S.Y. Choi, Fabrication of Cu-coated TiO_2 nanotubes and enhanced electrochemical performance of lithium ion batteries, J. Electroanal. Chem. 744 (2015) 45–52, http://dx.doi.org/10.1016/j.jelechem.2015.03.007.
[24] Y. Tang, X. Tan, G. Hou, G. Zheng, Nanocrystalline $Li_4Ti_5O_{12}$-coated TiO_2 nanotube arrays as three-dimensional anode for lithium-ion batteries,

Electrochim. Acta 117 (2014) 172–178, http://dx.doi.org/10.1016/j.electacta.2013.11.095.
[25] B. Ding, L. Shen, G. Xu, P. Nie, X. Zhang, Encapsulating sulfur into mesoporous TiO_2 host as a high performance cathode for lithium-sulfur battery, Electrochim. Acta 107 (2013) 78–84, http://dx.doi.org/10.1016/j.electacta.2013.06.009.
[26] X. Qian, X. Yang, L. Jin, D. Rao, S. Yao, X. Shen, K. Xiao, S. Qin, J. Xiang, High rate lithium-sulfur batteries enabled by mesoporous TiO_2 nanotubes prepared by electrospinning, Mater. Res. Bull. 95 (2017) 402–408, http://dx.doi.org/10.1016/j.materresbull.2017.07.009.
[27] S. Evers, T. Yim, L.F. Nazar, Understanding the nature of absorption/adsorption in nanoporous polysulfide sorbents for the Li-S battery, J. Phys. Chem. C 116 (2012) 19653–19658, http://dx.doi.org/10.1021/jp304380j.
[28] Z.W. Seh, W. Li, J.J. Cha, G. Zheng, Y. Yang, M.T. McDowell, P.C. Hsu, Y. Cui, Sulphur-TiO_2 yolk-shell nanoarchitecture with internal void space for long-cycle lithium-sulphur batteries, Nat. Commun. 4 (2013), http://dx.doi.org/10.1038/ncomms2327.
[29] H. Wang, S. Li, D. Li, Z. Chen, H.K. Liu, Z. Guo, TiO_2 coated three-dimensional hierarchically ordered porous sulfur electrode for the lithium/sulfur rechargeable batteries, Energy 75 (2014) 597–602, http://dx.doi.org/10.1016/j.energy.2014.08.029.
[30] K. Xie, K. Zhang, Y. Han, K. Yuan, Q. Song, J.G. Wang, C. Shen, X. Liu, B. Wei, A novel TiO_2-wrapped activated carbon fiber/sulfur hybrid cathode for high performance lithium sulfur batteries, Electrochim. Acta 210 (2016) 415–421, http://dx.doi.org/10.1016/j.electacta.2016.05.172.
[31] G.L. Holleck, J.R. Driscoll, Transition metal sulfides as cathodes for secondary lithium batteries-II. Titanium sulfides, Electrochim. Acta 22 (1977) 647–655, http://dx.doi.org/10.1016/0013-4686(77)85134-7.
[32] Y. Onuki, R. Inada, S. Tanuma, S. Yamanaka, H. Kamimura, Electrochemical characteristics of transition-metal trichalcogenides in the secondary lithium battery, Solid State Ionics 11 (1983) 195–201, http://dx.doi.org/10.1016/0167-2738(83)90024-3.
[33] M.H. Lindic, H. Martinez, A. Benayad, B. Pecquenard, P. Vinatier, A. Levasseur, D. Gonbeau, XPS investigations of TiO_ySz amorphous thin films used as positive electrode in lithium microbatteries, Solid State Ionics 176 (2005) 1529–1537, http://dx.doi.org/10.1016/j.ssi.2005.04.007.
[34] N.A. Kyeremateng, N. Plylahan, A.C.S. Dos Santos, L.V. Taveira, L.F.P. Dick, T. Djenizian, Sulfidated TiO_2 nanotubes: a potential 3D cathode material for Li-ion micro batteries, Chem. Commun. 49 (2013) 4205–4207, http://dx.doi.org/10.1039/c2cc36857a.
[35] M.H. Lindic, B. Pecquenard, P. Vinatier, A. Levasseur, H. Martinez, D. Gonbeau, P.E. Petit, G. Ouvrard, Electrochemical mechanisms during lithium insertion into $TiO_{0.6}S_{2.8}$ thin film positive electrode in lithium microbatteries, J. Electrochem. Soc. 152 (2005) A141, http://dx.doi.org/10.1149/1.1834893.
[36] M.S. Whittingham, The role of ternary phases in cathode reactions, J. Electrochem. Soc. 123 (1976) 315, http://dx.doi.org/10.1149/1.2132817.
[37] M.S. Whittingham, Electrical energy storage and intercalation chemistry, Science (80-.) 192 (1976) 1126–1127, http://dx.doi.org/10.1126/science.192.4244.1126.
[38] M.S. Whittingham, Chemistry of intercalation compounds: metal guests in chalcogenide hosts, Prog. Solid State Chem. 12 (1978) 41–99, http://dx.doi.org/10.1016/0079-6786(78)90003-1.
[39] B. Fleutot, B. Pecquenard, F. Le Cras, B. Delis, H. Martinez, L. Dupont, D. Guy-Bouyssou, Characterization of all-solid-state Li/LiPONB/TiOS microbatteries produced at the pilot scale, J. Power Sources 196 (2011) 10289–10296, http://dx.doi.org/10.1016/j.jpowsour.2011.07.018.
[40] M.H. Lindic, B. Pecquenard, P. Vinatier, A. Levasseur, H. Martinez, D. Gonbeau, P.E. Petit, G. Ouvrard, Characterization of rf sputtered TiO_ySz thin films, Thin Solid Films 484 (2005) 113–123, http://dx.doi.org/10.1016/j.tsf.2005.02.014.
[41] A. Hayashi, T. Matsuyama, A. Sakuda, M. Tatsumisago, Amorphous titanium sulfide electrode for all-solid-state rechargeable lithium batteries with high capacity, Chem. Lett. 41 (2012) 886–888, http://dx.doi.org/10.1246/cl.2012.886.
[42] H. Sopha, L. Hromadko, K. Nechvilova, J.M. Macak, Effect of electrolyte age and potential changes on the morphology of TiO_2 nanotubes, J. Electroanal. Chem. 759 (2015) 122–128, http://dx.doi.org/10.1016/j.jelechem.2015.11.002.
[43] R. Zazpe, M. Knaut, H. Sopha, L. Hromadko, M. Albert, J. Prikryl, V. Gärtnerová, J.W. Bartha, J.M. Macak, Atomic layer deposition for coating of high aspect ratio TiO_2 nanotube layers, Langmuir 32 (2016) 10551–10558, http://dx.doi.org/10.1021/acs.langmuir.6b03119.
[44] C.G. Hawkins, L. Whittaker-Brooks, Controlling sulfur vacancies in TiS_{2-x} cathode insertion hosts via the conversion of TiS_3 nanobelts for energy-storage applications, ACS Appl. Nano Mater. 1 (2018) 851–859, http://dx.doi.org/10.1021/acsanm.7b00266.
[45] B. Ding, C. Yuan, L. Shen, G. Xu, P. Nie, X. Zhang, Encapsulating sulfur into hierarchically ordered porous carbon as a high-performance cathode for lithium-sulfur batteries, Chem. A Eur. J. 19 (2013) 1013–1019, http://dx.doi.org/10.1002/chem.201202127.
[46] M. Barawi, E. Flores, M. Ponthieu, J.R. Ares, F. Cuevas, F. Leardini, I.J. Ferrer, C. Sánchez, Hydrogen storage by titanium based sulfides, J. Electr. Eng. 3 (2015) 24–29, http://dx.doi.org/10.17265/2328-2223/2015.01.004.
[47] A.J. Molina-Mendoza, J.O. Island, W.S. Paz, J.M. Clamagirand, J.R. Ares, E. Flores, F. Leardini, C. Sánchez, N. Agraït, G. Rubio-Bollinger, H.S.J. van der Zant, I.J. Ferrer, J.J. Palacios, A. Castellanos-Gomez, High current density electrical breakdown of TiS_3 nanoribbon-based field-effect transistors, Adv. Funct. Mater. 27 (2017) 1605647, http://dx.doi.org/10.1002/adfm.201605647.
[48] G.A. Muller, J.B. Cook, H. Kim, S.H. Tolbert, B. Dunn, High performance pseudocapacitor based on 2D layered metal chalcogenide nanocrystals, Nano Lett. 15 (2015) 1911–1917, http://dx.doi.org/10.1021/nl504764m.
[49] J.R. González, E. Zhecheva, R. Stoyanova, D. Nihtianova, P. Markov, R.R. Chapuis, R. Alcántara, F. Nacimiento, J.L. Tirado, G.F. Ortiz, A fractal-like electrode based on double-wall nanotubes of anatase exhibiting improved electrochemical behaviour in both lithium and sodium batteries, Phys. Chem. Chem. Phys. 17 (2015) 4687–4695, http://dx.doi.org/10.1039/c4cp04572f.
[50] J.M. Whiteley, S. Hafner, S.S. Han, S.C. Kim, V.-D. Le, C. Ban, Y.H. Kim, K.H. Oh, S.-H. Lee, J. Mater. Chem. A 5 (2017) 15661–15668, http://dx.doi.org/10.1039/C7TA03756B.
[51] D. Bauer, A.J. Roberts, N. Matsumi, J.A. Darr, Nano-sized Mo-and Nb-doped TiO_2 as anode materials for high energy and high power hybrid Li-ion capacitors, Nanotechnology 28 (2017) 195403, http://dx.doi.org/10.1088/1361-6528/aa69df.
[52] S. Brutti, V. Gentili, P. Reale, L. Carbone, S. Panero, Mitigation of the irreversible capacity and electrolyte decomposition in a $LiNi_{0.5}Mn_{1.5}O_4$/nano-TiO_2 Li-ion battery, J. Power Sources 196 (2011) 9792–9799, http://dx.doi.org/10.1016/j.jpowsour.2011.08.022.
[53] C. Park, W. Chang, H. Jung, J. Kim, H. Sohn, Electrochemistry communications nanostructured Sn/TiO_2/C composite as a high-performance anode for Li-ion batteries, Electrochem. Commun. 11 (2009) 2165–2168, http://dx.doi.org/10.1016/j.elecom.2009.09.021.